Korean J. Chem. Eng., 35(2), 383-393 (2018)
DOI: 10.1007/s11814-017-0306-8

pISSN: 0256-1115
eISSN: 1975-7220

Effects of zirconia loading in sulfated zirconia/SBA-15 on esterification of palmitic acid with glycerol

Mohd Hizami Mohd Yusoff† and Ahmad Zuhairi Abdullah

School of Chemical Engineering, Engineering Campus, Universiti Sains Malaysia, 14300 Nibong Tebal, Penang, Malaysia
(*Received 4 May 2017 • accepted 5 November 2017*)

Abstract−Sulfated zirconia supported on SBA-15 (SZSBA-15) catalysts with different zirconia loadings (5-20 wt%) were synthesized using urea hydrolysis method. Effects on the physicochemical properties of the catalysts and activity in selective glycerol esterification with palmitic acid were particularly investigated. Various characterization techniques such as N_2 adsorption-desorption analysis, SEM, TEM, TGA, FTIR, NH_3-TPD and acidity measurement by titration were used. Increasing zirconia loading decreased the surface area, pore size and pore volume of the catalysts, but increased the sulfate content and improved the catalyst acidity. Larger surface area was not the major factor in determining the catalyst activity especially in the reaction involving bulky molecules. The reaction was found to be influenced by the amount of active sites presence on the catalyst and also by the dimension of the pores which slightly promoted the shape selective reaction. Among all catalyst, 15SZSBA-15 demonstrated the highest activity with 88% conversion and 44% monopalmitin yield.

Keywords: SBA-15, Sulfated Zirconia, Urea Hydrolysis, Selective Esterification, Monopalmitin

INTRODUCTION

Recently, there has been a growing research interest in the application of monoglyceride as an emulsifier in food, pharmaceutical and cosmetics industries [1]. Among them, food industry is considered as a fastest growing segment of food additives because of the increasing trend towards reducing fat content in food products for consumer health benefits. Due to rising health concerns, the increasing demand for low-fat foods would subsequently drive the demand for emulsifier. Based on the current trend, emulsifier market is expected to reach volume sales of 2.6 million metric tons by 2017 [2].

Monoglycerides are commercially synthesized via acid catalyzed esterification of glycerol with various types of fatty acids to produce monolaurin [3], monoolein [4,5] and monostearin [6]. Meanwhile, palmitic acid has become a potential choice for monopalmitin synthesis, as this value-added product can be obtained from a low value feedstock such as palm oil. Conventionally, esterification reactions are carried out in the presence of homogeneous acid catalysts, i.e., sulfuric acid [7-9], hydrochloric acid [10] and phosphoric acid [11]. However, the catalyst poses significant drawbacks that could reduce the efficiency of the process such as generation of polluting by-products, large energy consumption, high cost separation, toxicity and corrosiveness [12]. Furthermore, a number of solid acid catalysts, i.e., ion-exchange resins [13] and zeolite [14], have also been developed for this purpose. Amberlyst IR-120 with a surface area of 0.3 m^2/g has been used in the production of monolaurin and 98% of lauric acid conversion was obtained [13]. Although the conversion was significantly high, the catalyst without porosity only favored the formation of diglyceride which was measured to be 100%. Meanwhile, high selectivity of monoolein (55%) was obtained using ultra stable Y-zeolite in the reaction involving glycerol and oleic acid [14]. However, the monoolein yield was low, and this was attributed to the small pore diameter which restricted the diffusion of bulky molecules into the porous channels of zeolites [15]. Several studies have also been conducted on the production of monopalmitin using enzymes [1,16]. However, the enzymatic process is inefficient due to its reusability issues and requires longer reaction time to achieve high conversion [17]. Therefore, the application of heterogeneous superacid catalysts that are stable, regenerable and selective towards monoglyceride is needed. Sulfated zirconia (SZ) supported on SBA-15 (SZSBA-15) is a potential catalyst due to its strong acidic nature, high surface area, large pore volume and uniform pores, which is beneficial in the reaction involving bulky reactants. Despite showing high activity in many reactions including oxybromination [18], cellobiose hydrolysis [19] and cumene cracking [20], SZSBA-15 exhibited high catalytic activity in the production of monopalmitin via glycerol esterification with palmitic acid [21]. The high catalytic activity was attributed to the high density of active acid sites in the catalyst.

Sulfated zirconia is known to possess both strong Brønsted and Lewis acid sites on the surface [22]. Therefore, dispersion of sulfated zirconia particles on the large surface area of SBA-15 should greatly enhance the acidity and physical properties of the catalyst. Catalyst acidity plays an important role in the esterification reaction and it is influenced by various factors such as the preparation method and calcination temperature [23]. As for the preparation method, the initial amount of zirconia is generally found to influence the textural properties, final acidity of the catalyst and its performance. Krishnan et al. [24] synthesized SBA-15 coated with

†To whom correspondence should be addressed.
E-mail: jami053@yahoo.com

zirconia via vapor-induced internal hydrolysis (VIH) method and found that the increase in the dispersion of zirconium species enhanced the acidity of the catalyst. Degirmenci et al. [25] found that 25 mol% ZrO_2 included SBA-15 catalyst with a BET surface area of 246 m^2/g exhibited the highest acidity. Garg et al. [20] reported that the sulfate content passed through a maximum after being loaded with 35 wt% ZrO_2 loading and the catalyst having pore size of 45 Å showed high activity towards cumene cracking. However, the role of pore characteristics in the selective reaction was not emphasized. Limited information has been reported on the effect of zirconia loading on the physical and chemical characteristic of SZSBA-15. Furthermore, no work has been reported so far on the effect of zirconia loadings on the mono-, di-, and tripalmitin selectivities from the reaction of glycerol with palmitic acid.

Dispersion of large amount of zirconia inside SBA-15 could alter the surface and textural properties of the catalyst which limits the accessibility of bulky reactants. Therefore, modifications of surface properties with zirconia loadings while optimizing the catalyst acidity is vital to ensure high catalytic activity towards the formation of monoglycerides. In this study, the amount of zirconia (5, 15 and 20 wt%) in the SZSBA-15 was varied and used in the reaction to produce monopalmitin. The objectives of the present work were to study the changes in the physicochemical and morphological properties of catalysts and to investigate the effects on the activity and products distribution from the reaction of palmitic acid and glycerol. Correlations between the physicochemical properties and catalytic activity in the reaction involving glycerol and palmitic acid are elucidated. Thus, an understanding on the relation between the physicochemical properties of SZSBA-15 catalyst in the selective reaction of glycerol with palmitic acid has been established.

EXPERIMENTAL

1. Catalyst Preparation

SBA-15 and SZSBA-15 catalysts were synthesized according to our previous work [21]. For variation of zirconia loading (5-20 wt%), the catalysts were prepared as discussed in the published work with appropriate amounts of zirconia precursor. For example, SZSBA-15 catalysts with 5 wt% of zirconia loading (5SZSBA-15) was prepared by the addition of 0.2753 g of $ZrOCl_2{\cdot}8H_2O$ into 120 mL of distilled water containing 1.083 g of urea. Their corresponding loadings are designated as *x*SZSBA-15 where *x* stands for the theoretical wt% of ZrO_2 in SBA-15.

2. Catalyst Characterization

The textural analysis was carried out using a Micromeritics ASAP 2020 equipment. Scanning electron microscopy (SEM) images were captured using a Quanta FEG 450 SEM and EDX analysis was performed using the same equipment. The transmission electron microscope (TEM) images were recorded by means of a Philips CM12 TEM microscope at an accelerating voltage of 120 kV. The FTIR spectra of the samples were recorded by means of a Perkin Elmer 2000 system using KBr pellet technique. The thermogravimetric analysis (TGA) was performed using a Perkin Elmer (TGA7) thermogravimetric analyzer with N_2 gas flow rate of 20 ml/min and the heating rate of 10 °C/min from 25 to 800 °C. The acidic strength of the catalysts was measured using temperature-programmed desorption of ammonia (NH_3-TPD) using a Micromeritics AutoChem II 2920 instrument. In a typical experiment, 0.1 g of sample was pretreated at 110 °C in flowing He for 1 h. The NH_3 adsorption was then carried out at 120 °C, and desorption of NH_3 was started at 120 °C and further continued until 600 °C at 10 °C/min. Meanwhile, the surface acidity was quantitatively estimated using HCl titration [26]. In this determination, 0.5 g of catalyst was added into 15 mL NaOH (0.1 M) and stirred for 1 h. Then the catalyst was filtered and the remaining solution was titrated with HCl (0.1 M) with phenolphthalein indicator.

3. Esterification of Glycerol with Palmitic Acid and Product Analysis

Palmitic acid (0.0585 mol), glycerol (0.2340 mol) and 2 wt% of the catalyst (with respect to palmitic acid) were added into a 250 mL three-necked round bottom flask, heated to 170 °C and stirred for 3 h under a continuous nitrogen flow of 10 cm^3/min. Esterification reactions were performed in triplicate to ensure good empirical reproducibility. For product analysis, 200 μL sample was added into 200 μL water and 200 μL methyl acetate [21]. The mixture was vortexed, centrifuged and 40 μL of the top layer was diluted with 1,000 μL acetone and 100 μL internal standards (10 mg/ml of n-tetradecane in acetone). 1 μL of the solution was then injected into a gas chromatograph (Agilent 7820A) equipped with a CP Sil 5CB capillary column (15 m×0.32 mm×0.10 μm). The temperature of the column was held at 80 °C for 1 min, increased to 340 °C at a rate of 10 °C/min and maintained for 5 min. The temperatures of the injector and detector were 250 and 310 °C, respectively. The conversion of palmitic acid and selectivity of the respective glycerides were calculated based on a published method [27].

RESULTS AND DISCUSSION

1. Catalyst Characterization

1-1. Physicochemical Properties of Catalysts

The physicochemical properties of the SBA-15 support and SZSBA-15 catalysts prepared at different zirconia loadings (5, 15 and 20 wt%) are presented in Table 1. After incorporating SBA-15 with increasing zirconia loading, the surface area of SZSBA-15 catalysts significantly decreased. This could be attributed to the increase in the amount of zirconia on the SBA-15, which consequently led to the partial collapse of the mesoporous structure. Similar trend was observed in the pore volume to suggest that some of the sulfated zirconia species was successfully loaded into the mesoporous support [22]. Furthermore, at high zirconia loading, more active phase are available to accommodate the porous channels. Thus, most of the pores on the SBA-15 were occupied, which led to the lower pore volume. Moreover, the SZSBA-15 catalysts showed both lower mesopore and micropore areas compared to that of the pristine SBA-15.

By increasing the zirconia loading from 5 to 20 wt%, the pore diameter was found to decrease from 76 to 57 Å, indicating rather severe pore blockage due to the formation of zirconia deposits on the pore surface. However, the pore diameters of all catalysts except 20SZSBA-15 were larger than that of the pristine SBA-15. This finding suggests the influence of zirconia loadings used during the

synthesis on the dispersion of zirconia on the SBA-15 [28]. At low loading, the zirconia particles were mainly dispersed at the mouth of the mesopores that would lead to the partial collapse of pore wall. On the other hand, the dispersion of higher loading zirconia followed a dual-step filling. The first stage of dispersion also occurred at the mouth of the mesopores, while the second stage occurred inside the channels and filling the microporous channels, which consequently decreased the pore diameter. Similar finding on the enlargement of pore diameter during synthesis was also reported in a previous work [27]. Meanwhile, for 20SZSBA-15, higher loading of zirconia might have blocked the mesopores of SBA-15, which resulted in lower surface area. On the other hand, the pore diameter was roughly the same as that of SBA-15. Despite having the same pore diameter, the pore volume of the 20SZSBA-15 was much smaller than SBA-15, which suggests the significant deposition of active zirconia particles inside the internal pores of SBA-15. Nevertheless, the pore sizes of all catalysts were in the meso range, which is important in for the transport of bulky molecules in liquid-state catalysis [29].

The nitrogen adsorption-desorption isotherms for SBA-15 and SZSBA-15 catalysts are illustrated in Fig. 1(a). A decreasing trend of hysteresis loop is observed upon the introduction of zirconia with increasing loading, which reflects the decreasing pore volume. Nevertheless, all the isotherms possess type IV model with H1 type hysteresis loop, which are typical for materials having mesoporous channels [30]. This means that the hexagonal structures of the SBA-15 were not altered after being incorporated with zirconia particles with a loading of up to 20 wt%. Although the catalysts showed similar isotherms, the quantity of adsorbed nitrogen was found to be different for all catalysts. As shown in Fig. 1(a), SBA-15 had high adsorption capacity exceeding 580 cm^3/g STP. However, the increase in zirconia loading decreased the quantity of adsorbed nitrogen. Among all the catalysts, higher nitrogen adsorption exceeding 450 cm^3/g STP was observed for the catalyst prepared using 5 wt% of zirconia. As for the 15 wt% catalyst, the amount of the adsorbed nitrogen significantly dropped to 350 cm^3/g STP, implying the reduction of pore volume as a result of pore plugging. On the other hand, 20 wt% of zirconia loading caused the most significant decrease in the quantity of adsorbed nitrogen, which was around 200 cm^3/g STP. The poor adsorption property of the catalyst was attributed to the reduction in the surface area and pore volume as shown in Table 1; this consequently affected the molecular transport of bulky molecules in the esterification reaction.

Fig. 1(b) shows the BJH pore size distribution for SBA-15 and the catalysts. The figure provides strong evidence on the reduction of pore size with increasing zirconia loading. It can be observed that the incorporation of 5 wt% of zirconia on SBA-15 resulted in a broader pore distribution and the peak shifted to higher pore diameter with a maximum peak of 76 Å. However, the pore size distribution shifted to smaller pore sizes with further increase in the zirconia loading. The decrease in the pore size was due to the partial coating of zirconia layer on the pore surface as a result of deposition of large amount of zirconia [31]. Furthermore, narrow pore size distributions were obtained for 15SZSBA-15 and 20SZSBA-15, while broader distribution was observed for 5SZSBA-15.

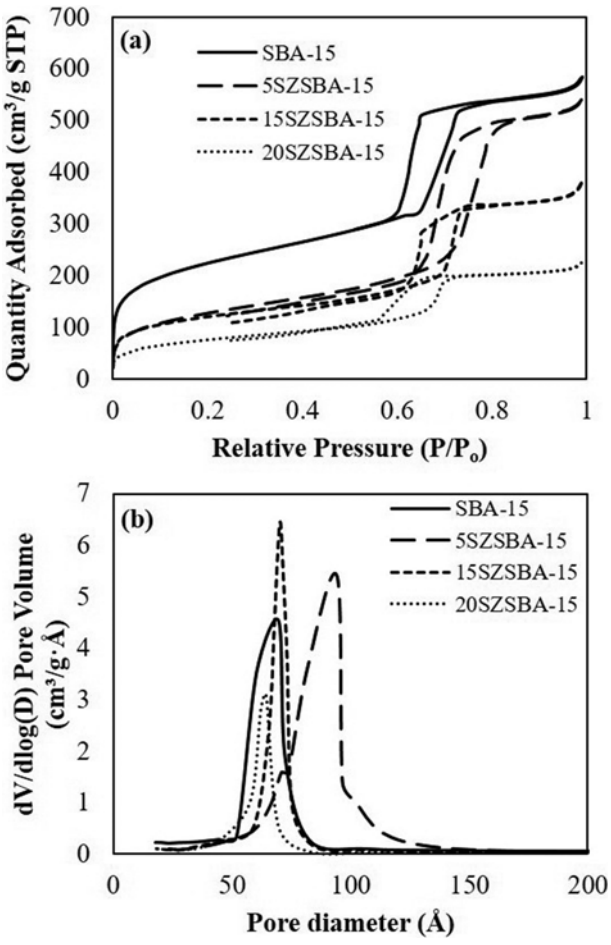

Fig. 1. The profiles of (a) N_2 adsorption-desorption isotherm and (b) pore size distribution of SBA-15 support and catalysts.

The zirconia and sulfur content on the catalysts are presented in Table 2. The amounts of zirconia on the calcined products were lower than the theoretical amounts in the synthesis gel. This finding indicated that not all of zirconia had been successfully incorporated into the SBA-15 framework, and the remaining zirconia could remain dissolved in the synthesis solution [19]. However,

Table 1. Physical properties of the support and catalysts

Material	Surface area (m^2/g)	Mesopore area (m^2/g)	Micropore area (m^2/g)	Pore volume (cm^3/g)	Pore diameter (Å)
SBA-15	769	604	165	0.89	57
5SZSBA-15	445	427	18	0.88	76
15SZSBA-15	414	336	78	0.57	67
20SZSBA-15	264	243	21	0.34	57

Table 2. Chemical properties of the support and catalysts

Catalyst	Zr content (wt%)	Sulfur content (wt%)	Acidity	
			HCl titration (mmol/g)	NH_3-TPD (mmol/g)
SBA-15	-	-	0.10	0.01
5SZSBA-15	2.75	0.46	2.08	1.64
15SZSBA-15	9.11	2.06	2.58	2.73
20SZSBA-15	9.38	2.18	2.32	2.01

the amount of zirconia was found to influence the attachment of sulfur on the catalyst. The sulfur content increased with increasing zirconia loading; however, the sulfur content on the catalyst did not change much with increasing zirconia loading from 15 to 20 wt%. This is due to the dispersion of zirconia on the external surface of SBA-15, which limited the sulfation process to only on the outer surface of catalyst.

Table 2 also compares the acidity of the SZSBA-15 catalysts

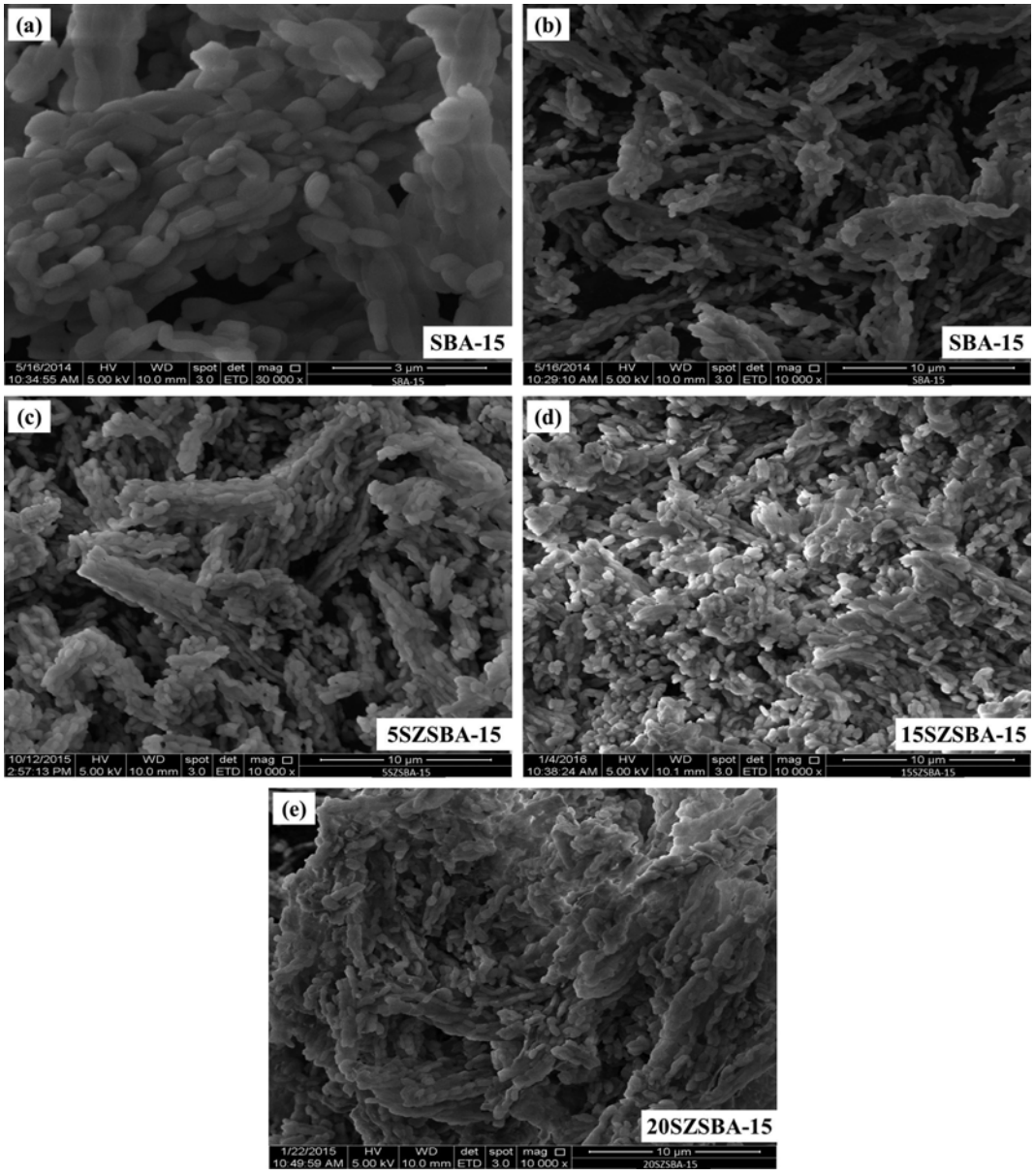

Fig. 2. SEM images of (a) SBA-15 at magnification of 30000×, (b) SBA-15 at a magnification of 10000×, (c) 5SZSBA-15, (d) 15SZSBA-15 and (e) 20SZSBA-15.

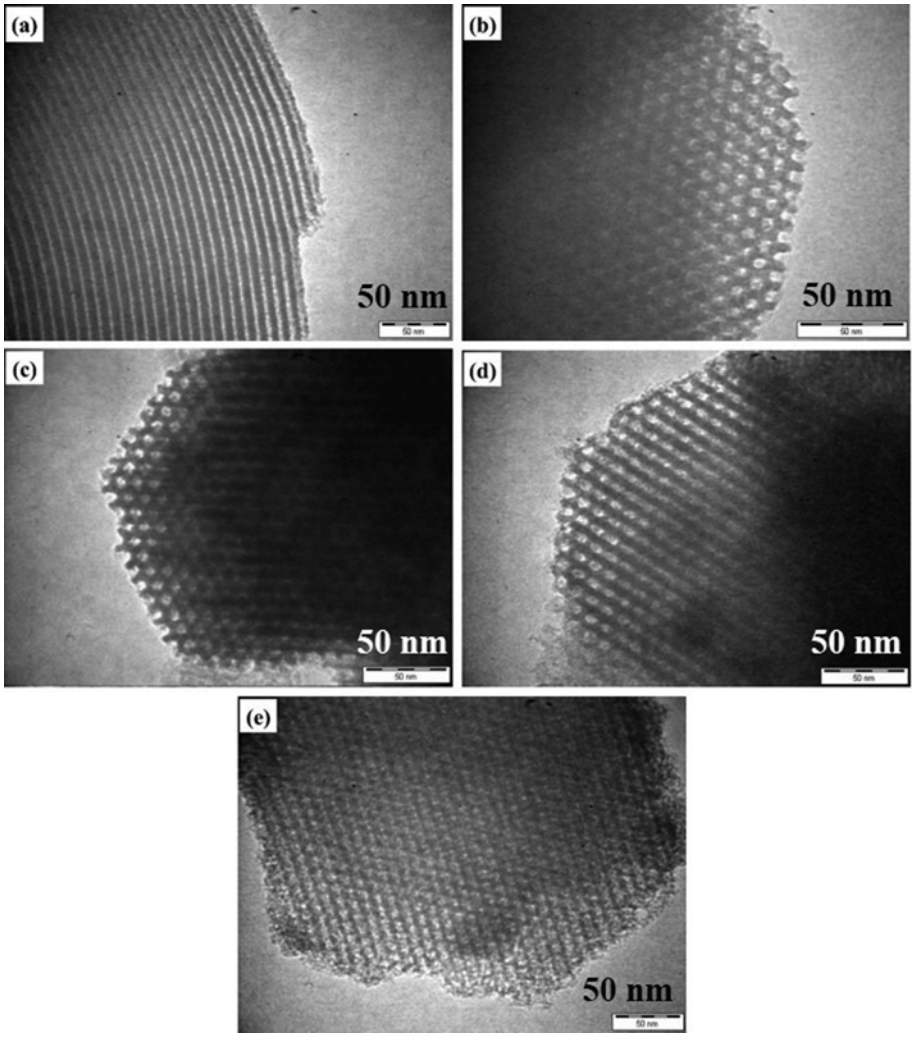

Fig. 3. TEM images of (a) SBA-15 in the direction perpendicular to the pore axis, (b) SBA-15 in the direction of the pore axis, (c) 5SZSBA-15, (d) 15SZSBA-15 and (e) 20SZSBA-15 catalysts.

obtained from HCl titration method and NH_3-TPD analysis. Interestingly, increasing zirconia loading also increased the acidity of the catalysts as a result of high sulfur content. Low acid density was observed for 5SZSBA-15 due to the small amount of sulfur presence on the catalyst. Meanwhile, the acidity of 15SZSBA-15 catalyst was the highest as a result of high sulfur content. These findings could be related to the types of acid site (Lewis and Brønsted) on the surface of the catalyst. At lower and higher sulfur content, the surface of the catalysts mainly contained weak acid sites (Lewis acid) and strong acid sites (Brønsted acid) [32]. However, no significant change was observed in the acidity of 20SZSBA-15 catalyst. This result suggests that further increases in zirconia loading would no longer increase the acidity but possibly reduce the density of acid sites instead. Similar trend was also observed for the acidity of the catalysts obtained from the NH_3-TPD analysis in which the number of acid sites determined by this method passed through a maximum for 15SZSBA-15 catalyst.

1-2. Morphological Structure

The SEM and TEM images of the SBA-15 and SZSBA-15 catalysts prepared at different zirconia loadings (5-20 wt%) are depicted in Fig. 2 and Fig. 3, respectively. The SEM images reveal that the SBA-15 morphology appeared as a chain of rope-like domain (Fig. 2(a)) with uniform sizes of roughly 1 μm, which aggregated into a wheat-like macrostructures (Fig. 2(b)). Similar structure was also observed by other researcher [33] indicating successful synthesis of the mesoporous SBA-15 material.

The increase in the zirconia loading was found to give significant effect on the surface morphology of the catalysts. After being loaded with 5 wt% of zirconia, the macrostructures agglomerated into larger domains (Fig. 2(c)). However, the voids between the wheat-like macrostructures are still visible at lower zirconia loading. As the zirconia loading was increased, the rope-like particles aggregated into a more dense materials (Fig. 2(d)-(e)). This could be due to the presence of high amount of zirconia species, which increased the possibility of attachment between ZrO_2 phase and the voids between the macrostructures. Furthermore, the individual sizes of the rope-like particles were found to be uniform for zirconia loading up to 15 wt% and no traces of zirconia layer was observed on the external surface of the catalysts. This finding indicates that the zirconia particles was successfully loaded into the

SBA-15 framework.

In the meantime, at higher loading (20 wt%), morphology of the catalyst slightly changed with the formation of zirconia layer on the surface of the rope-like structure. As shown in Fig. 2(e), 20SZSBA-15 exhibited large aggregated particles with irregular structures and formed crystal-like macrostructures. This was due to the deposition of large amount of zirconia within the porous channels and also on the surface of the SBA-15 channels. This consequently reduced the surface area, pore volume and diameter, as confirmed from the textural analysis. Even so, the original morphology of the SBA-15 was retained for all catalysts.

Fig. 3 presents the TEM images of the SBA-15 and catalysts with different loadings (5-20 wt%). Fig. 3(a) and 3(b) depict the TEM images of SBA-15 in the direction perpendicular and in the direction of the pore axis, respectively. It can be seen that the synthesized SBA-15 exhibits well-ordered hexagonal arrays of uniform mesopores and the typical honeycomb, resembling to that of conventional SBA-15. After the addition of sulfated zirconia, dark spots were observed for all the catalysts, which indicates the incorporation of zirconia particles on the mesoporous SBA-15. As can be visually observed in Fig. 3(c)-(e), the pore channels enlarged after the addition of 5 wt% of zirconia, but decreased with further increase in zirconia loading. At higher zirconia loading of 20 wt%, it is clearly shown that the zirconia particles accommodated both inner and outer surfaces of the SBA-15. Furthermore, agglomerated excess zirconia particles were found to disperse on the outer surface of the silica materials (Fig. 3(e)). As a result, the pore volume and pore diameter of 20SZSBA-15 catalyst significantly decreased compared to those of the other catalysts. This observation was consistent with the surface characteristics as obtained from the nitrogen adsorption-desorption analysis. Nevertheless, the original hexagonal structure of SBA-15 was preserved after the incorporation of zirconia with subsequent sulfation, which indicates that the catalyst could be prepared at higher loading without affecting the ordered mesostructure. Therefore, from the SEM and TEM images, it can be concluded that the morphology of the catalyst was stable and could be prepared at higher zirconia loadings of up to 20 wt% without significant alteration on the original morphology of SBA-15 as well as its mesostructures.

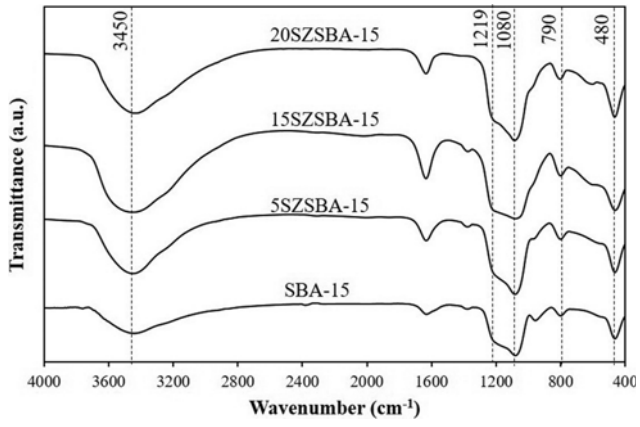

Fig. 4. FTIR spectra of SBA-15 and catalysts prepared at different zirconia loadings between 4,000-400 cm^{-1}.

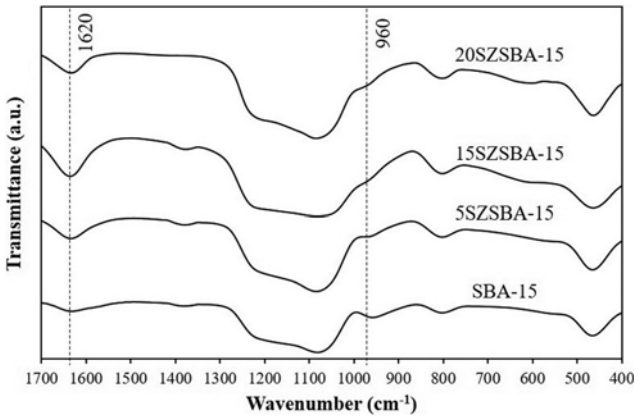

Fig. 5. FTIR spectra of SBA-15 and catalysts prepared at different zirconia loadings between 1,700-400 cm^{-1}.

1-3. FTIR

The FTIR spectra of the SBA-15 and SZSBA-15 catalysts in the framework region of 4,000-400 cm^{-1} are presented in Fig. 4. The vibration bands at 480, 790 and 1,080 cm^{-1} are observed in all samples, indicating the bending vibration of Si-O-Si, symmetric stretching of Si-O-Si and asymmetric stretching of Si-O-Si, respectively, which are usually present in SBA-15. This result suggests the ability of the support to maintain the silica framework even after the incorporation of sulfated zirconia. Additionally, the band at 1,080 cm^{-1} with a shoulder at about 1,219 cm^{-1} becomes more intense and broad after the addition of zirconia. The changes in the band intensities indicate the presence of chelating bidentate sulfur ions coordinated to zirconia cation, and the peaks are merged within the region of 1,219-1,058 cm^{-1} [34]. The merging of the sulfur peaks was also found in the sulfated ZrO_2-SiO_2 mixed oxide aerogel catalyst as reported by Saravanan et al. [35]. Meanwhile, the broad and intense band at 3,450 cm^{-1} is observed in all samples, which could be assigned to the stretching vibrations OH and Si-OH bonds [36].

Fig. 5 shows the detailed FTIR spectra of all samples in the framework region of 1,700-400 cm^{-1}. The vibration bands with different intensities at 960 and 1,620 cm^{-1} are observed in all samples. After the introduction of zirconia, the intensity of IR band at 960 cm^{-1} decreases, which could be possibly due to the stretching mode of [SiO_4] unit bonded to heteroatoms [37]. As the zirconia loading is further increased to 20 wt%, the peak disappears completely, indicating that the introduction of Zr^{4+} ions into the silica framework broke down its network. The disappearance of the band could be associated with Si-OH and Zr-OH that group to Si-O-Zr groups [31]. As the number of Si-O-Zr groups increased, the silanol groups would reduce. Meanwhile, increasing of zirconia loading from 5 to 15 wt% resulted in an increase in the band intensities at 1,620 cm^{-1}. An intense peak at this band is observed for 5SZSBA-15 and 15SZSBA-15 catalysts, which are attributed to O-H bending mode of water [36]. As for 20 wt% of zirconia loading, the intensity of the peak was found to decrease due to the availability of Si-OH in the SBA-15 support which was lower compared to the other catalysts.

1-4. TGA

The TGA profiles of the SBA-15 and SZSBA-15 catalysts are

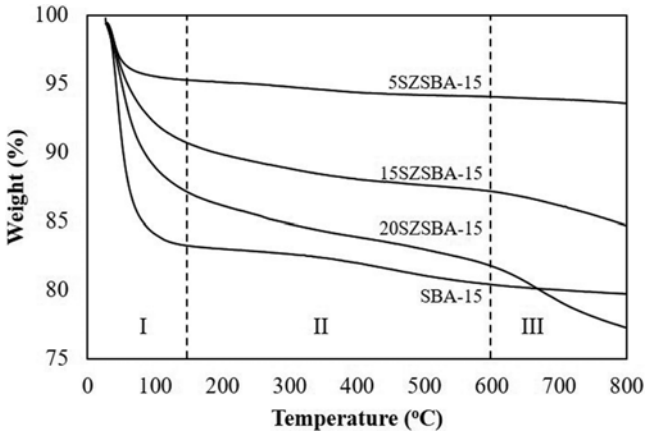

Fig. 6. TGA profiles of SBA-15, 5SZSBA-15, 15SZSBA-15 and 20SZSBA-15 catalysts.

presented in Fig. 6. SBA-15 shows two stages of weight loss when it was heated from room temperature to 800 °C under nitrogen flow. The first major weight loss of about 17 wt% occurred between 25 and 150 °C. This is attributed to the elimination of physisorbed water molecules on the surface of the support. High moisture content was adsorbed by SBA-15 due to its surface characteristics, which is hydrophilic [29]. The second decomposition stage appears between 200 and 600 °C with 2.6 wt% weight loss. This may be due to the condensation reaction between the Si-OH groups [38]. No significant weight loss was observed after that, implying that the SBA-15 support is stable up to 800 °C.

As for the other catalysts, three stages of thermal decomposition were observed. A significant weight loss also occurred between 25 to 150 °C due to the loss of adsorbed water. 20SZSBA-15 showed the highest weight loss (12 wt%) followed by 15SZSBA-15 (9 wt%) and 5SZSBA-15 (5 wt%). This finding indicates that the increase in the zirconia loading increased the hydrophilicity of catalysts, which might be beneficial in the reaction that produces water as the byproduct. The second weight loss appears between 150 and 600 °C. The gradual weight loss was probably due to the decomposition of organic residue or contaminants during the high temperature treatment. The third stage of weight loss occurred at around 600 to 800 °C due to decomposition of sulfates [39]. Within this temperature range, $Zr(SO_4)_2$ was more likely to decompose into ZrO_2 and SO_3. Weight loss at this stage increased notably with the increase in the zirconia loading. For example, 5SZSBA-15 showed the lowest weight loss (0.5 wt%) followed by 15SZSBA-15 (3.92 wt%) and 20SZSBA-15 (4.53 wt%). This is due to the high content of sulfur in the catalyst at high zirconia loadings, as confirmed by EDX analysis.

1-5. NH_3-TPD

The profile of NH_3-TPD for SZSBA-15 catalysts with different zirconia loadings (5-20 wt%) is shown in Fig. 7. From the figure, all synthesized catalysts show similar trend of NH_3 desorption profiles with four desorption peaks. These peaks could be associated with the formation of weak, moderate and strong acid strength, which generally occurred at low temperature region (<200 °C), intermediate temperature (between 200 and 450 °C) and high temperature region (more than 450 °C), respectively [40]. From the NH_3 desorption profiles, all catalysts showed maximum NH_3 desorption at the temperature region below 150 °C. This could be associated with the weak interaction between the NH_3 molecules

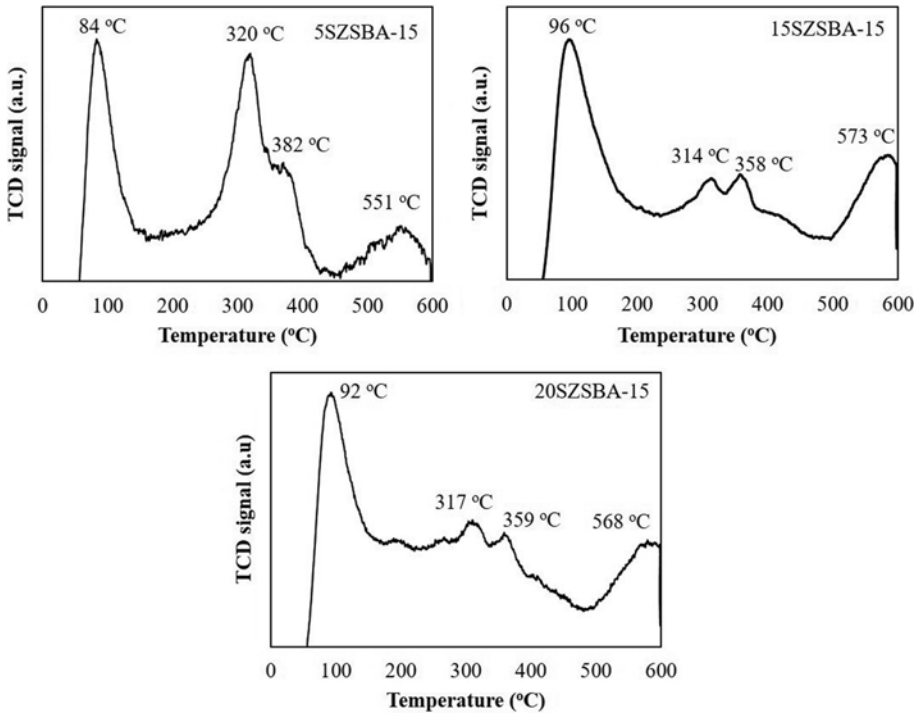

Fig. 7. NH_3-TPD profiles of 5SZSBA-15, 15SZSBA-15 and 20SZSBA-15 catalysts.

with the active sites located on the mouth of the mesopores [28]. Meanwhile, with an increase from 5 to 15 wt% of zirconia loading, the NH_3 desorption peak at high temperature region shifted to high values. The shifting in the NH_3 desorption peak temperature indicates an increase in the strength of the strong acid. At higher loading of 20 wt%, the desorption peaks slightly shifted to the lower values to suggest that the acid sites could have reached their maximum due to limited interaction between NH_3 molecules and the sulfated zirconium sites as a result of low surface area of the catalyst.

For 5SZSBA-15 catalyst, interestingly, the amount of desorbed NH_3 within 200 to 450 °C was the highest to indicate that the catalyst mainly consisted of weak and moderate acid strength. The higher amount of NH_3 desorbed could be associated to the uniform dispersion of zirconium species in the mesoporous channels, which consequently increased the number of coordinative unsaturated zirconium sites [24]. As a result, more NH_3 molecules could coordinate with the unsaturated zirconium sites. With further increase in the zirconia loading, the intensity of the peak within the intermediate temperature region significantly decreased due to the agglomeration of the primary particles at high zirconia loadings, which slightly reduced the concentration of active sites with intermediate strength. Nevertheless, two different peaks appeared within the temperature region of 314 °C to 385 °C, suggesting the presence of two types of sulfate species (i.e., pyrosulfate and monosulfate) [41]. Furthermore, the desorption peak for strong temperature slightly shifted to lower values upon increasing the zirconia loading from 15 to 20 wt%. Moreover, the amount of NH_3 desorbed also decreased to indicate a decrease in the acid strength. From the NH_3-TPD analysis, it can be concluded that an increase in the zirconia loading above 15 wt% would no longer increase the acid strength of the catalyst, especially in the strong temperature region. This finding is in agreement with the acidity obtained from the titration method as shown in Table 2. Above all, 15SZSBA-15 catalyst had the highest amount of strong acid sites compared to other catalysts. Nevertheless, the superacidity of the SZSBA-15 catalysts was proven from the appearance of the desorption peak at above 450 °C.

2. Catalytic Activity in Glycerol Esterification with Palmitic Acid

The prepared catalysts were used in glycerol esterification with palmitic acid. In this study, a glycerol to palmitic acid molar ratio of 4 was chosen since the excess of glycerol favors the formation of monoglyceride [3]. The activity of the catalysts was evaluated based on the conversion of palmitic acid, monopalmitin yield and its ability to promote selective reaction towards monopalmitin.

2-1. Effect on Palmitic Acid Conversion and Monopalmitin Yield

Effects of zirconia loading in the SZSBA-15 catalysts on the conversion and monopalmitin yield are shown in Fig. 8. The results show that the addition of SBA-15 in the reaction led to a conversion of 68%. Since the SBA-15 did not contain active sites, the activity was attributed to the autocatalytic reaction. Interestingly, the addition of SZSBA-15 catalysts significantly improved the catalytic activity. It was observed that increasing zirconia loading from 5 to 15 wt% increased the conversion of palmitic acid. However, the conversion decreased for the catalyst with 20 wt% of zirconia

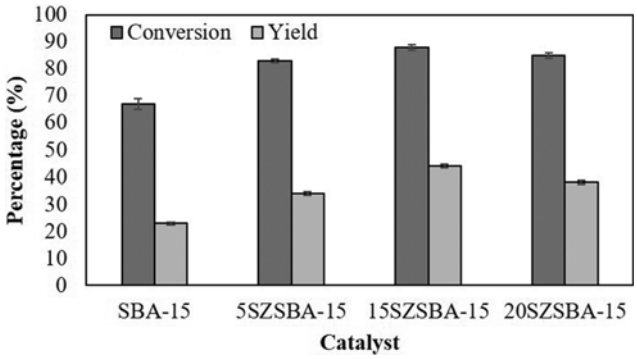

Fig. 8. Palmitic acid conversion and monopalmitin yield over SBA-15 and SZSBA-15 catalysts (Reaction temperature=170 °C, reaction time=3 h, glycerol/palmitic acid=4 : 1, catalyst loading=2 wt%).

loading. Nevertheless, all of the catalysts demonstrated high palmitic acid conversion ranging from 83 to 88% after 3 h of reaction. The insignificant differences in the conversion was due to the slight difference in the catalyst acidity which is in the range of 2.08 to 2.58 mmol/g, as shown in Table 2.

Despite its high surface area, 5SZSBA-15 showed the lowest conversion (83%) and monopalmitin yield (34%) compared to the other catalysts. This could be due to the low active acid sites available on the catalyst and also large pore size allowing the formation of byproducts (di- and tripalmitin) other than monopalmitin. Meanwhile, the conversion of palmitic acid increased by 5% using 15SZSBA-15 catalyst. Besides, the monopalmitin yield obtained using 15SZSBA-15 catalyst was 44%, which was 10% higher than that of 5SZSBA-15. This finding suggests the influence of the catalyst acidity and the pore characteristics that promote selective reaction towards the formation of monopalmitin.

On the contrary, further increase in zirconia loading decreased the palmitic acid conversion. Although the surface area of 20SZSBA-15 catalyst was lower compared to other catalysts, the significantly high conversion (85%) could be attributed to the presence of superacidic sites on the surface of the catalyst, which enhanced the rate of reaction. However, the monopalmitin yield was only 38%, suggesting that the formation of bulkier molecules such as di- and tripalmitin was more favorable using this catalyst. At higher loading, the presence of zirconia layer on the surface of the catalyst (as shown in SEM and TEM images) could have partially blocked the mesoporous channels, limited the accessibility of the reactants into the pores, and hindered the molecular interaction with the active sites. As a result, the reaction mostly occurred on the external surface of the catalyst, but under steric control [27].

2-2. Effect on Mono-, Di- and Tripalmitin Selectivities

Fig. 9 shows the product distribution for all catalysts. It was observed that mono-, di- and tripalmitin with different selectivities were generated using all catalysts including SBA-15. This result indicates that the reaction of palmitic acid under an excess of glycerol followed an irreversible parallel reactions. As a result, two or three hydroxyl groups from glycerol would also react with palmitic acid yielding di- and tripalmitin at the same time. Similar observation was also reported by Hermida et al. [27] in the reac-

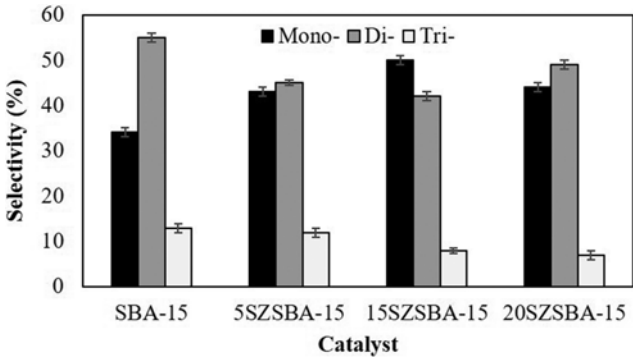

Fig. 9. Selectivity of monopalmitin, dipalmitin and tripalmitin over SBA-15 and SZSBA-15 catalysts (Reaction temperature= 170 °C, reaction time=3 h, glycerol/palmitic acid=4 : 1, catalyst loading=2 wt%).

tion involving lauric acid and glycerol under a continuous removal of water. Regardless of the autocatalytic reaction, high selectivity of di- and tripalmitin was observed with the addition of SBA-15. This could be due to the small pore size of SBA-15, which provided certain geometric constraints to the reactants and products [42]. On the contrary, the addition of SZSBA-15 catalyst was found to promote the selective reaction towards monopalmitin with high selectivity, while at the same time reduced the selectivity of dipalmitin. This could be attributed to the geometric constraints in the catalyst pores that minimized the diffusion of bulky reactants to form larger molecules [43]. However, low selectivity of tripalmitin (<12%) was also observed for all catalysts implying that the formation of this bulky molecule at high reaction temperature (170 °C) was unavoidable. Previous study has shown that the reaction of palmitic acid and glycerol conducted at 170 °C is practical from an economic standpoint [21].

For 5SZSBA-15 catalyst having pore size of 76 Å, there was not much difference between the selectivity of mono- and dipalmitin. This is due to the larger mesopores that allowed the reaction to form higher glycerides within the pores filled with active sites. Although large pores are more suitable to facilitate the reaction involving big molecules, the formation of higher glycerides would reduce the yield of the desired product i.e. monopalmitin. On the other hand, high selectivity of monopalmitin was obtained using 15SZSBA-15 having pore size of 67 Å. This result could be explained from the large amount of available mesopores as shown in the BJH pore distribution profile (Fig. 1(b)). This consequently increased the capacity to accommodate bulky molecules inside its porous structure with high degree of specificity.

On the other hand, a decrease in the monopalmitin selectivity was observed for 20SZSBA-15 having pore size of 57 Å. This was attributed to the smaller pore sizes of the catalyst that limited the diffusion of glycerol and palmitic acid molecules to form monopalmitin. Although the pore size is similar to that of pristine SBA-15, the porous channels are filled with active sites, which enhanced the reaction towards monopalmitin. Compared to other catalysts, 20SZSBA-15 produced more dipalmitin, and this could be attributed to the strong hydrophilicity of the catalyst surface [44]. This finding is in agreement with the result obtained from the TGA analysis. In addition, lower selectivity of tripalmitin (7%) was observed that could be attributed to the steric hindrance of the earlier attached reacting molecules [27]. Thus, the results suggest that 20SZSBA-15 catalyst with strong hydrophilicity only favored the formation of dipalmitin while the smaller pore size was responsible to the low monopalmitin selectivity.

From the catalytic activity, it was found that the conversion of palmitic acid to mono-, di- and tripalmitin was influenced by the acidity of the catalyst. The presence of high amount of active acid sites on the catalyst increased the potential collision between the reactants and active sites and hence, increased the conversion of palmitic acid. However, the yield of monopalmitin was influenced by the characteristics of the pores in which it directly affected the product distribution. For the reaction involving the formation of bulky molecules with different molecular sizes, pore dimension plays a crucial part to allow the formation of desired product with high selectivity. In this work, the different in the catalyst pore sizes with certain geometric constraint were responsible for the high selectivity of monopalmitin. Therefore, for this reaction involving a mesoporous solid acid catalyst like SZSBA-15, both acidity and pore dimension of the catalyst play important role to achieve high palmitic acid conversion with high monopalmitin yield.

3. Comparison of SZSBA-15 Performance with Other Solid Acid Catalysts

In a previous work by Abdullah et al. [32], high monolaurin yield (79.1%) was observed using SZSBA-15 having pore size of 64 Å. This result was indeed an expected one considering the shorter fatty acid chain length possesses by lauric acid (C12:0) compared to palmitic acid (C16:0). Thus, lower reaction temperature (160 °C) was sufficient to enhance the activity of the catalyst, which in turn increased the monolaurin yield. Meanwhile, Table 3 compares the performance of 15SZSBA-15 catalyst with other mesoporous silica based catalysts [3,27]. It was found that 15SZSBA-15 catalyst was the best catalyst in this work in which it required lower glycerol/fatty acid molar ratio, shorter reaction time and less amount of catalyst to achieve high yield. Although the yield obtained using HSO_3SBA-15 was high (68%), the amount of catalyst used was high and the reaction time was longer than this work. Thus, this catalyst has the potential to minimize the operating cost for monoglyceride production.

Table 3. Performance of SZSBA-15 and various reported mesoporous catalysts for monoglyceride production

Catalyst	Fatty acid	Product	Catalyst loading (wt%)	Glycerol/FA molar ratio	Time (h)	Yield (%)	References
15SZSBA-15	Palmitic acid	Monopalmitin	2.0	4 : 1	3	44	This work
20 wt%HPW/DS	Lauric acid	Monolaurin	2.5	4 : 1	3	25	[3]
HSO_3SBA-15	Lauric acid	Monolaurin	5.0	4 : 1	7	68	[27]

CONCLUSIONS

The effects of zirconia loading on the physicochemical properties of SZSBA-15 catalyst were successfully investigated by various characterization techniques. The incorporation of zirconia species on SBA-15 at different loadings (5, 15 and 20 wt%) was found to influence the textural properties, acidity, surface morphology and activity of the catalysts in glycerol esterification with palmitic acid. Increasing zirconia loading decreased the surface area, pore volume and pore size. Meanwhile, further increases in zirconia loading above 15 wt% would no longer increase the sulfur content, but possibly reduce the density of acid sites instead. The catalysts were stable and could be prepared at higher loadings of up to 20 wt% of zirconia without altering the original morphology of SBA-15 as well as its mesostructures. It was concluded that larger surface area was not the major factor in determining the catalyst activity, especially in the reaction involving this bulky molecule. The reaction was found to be influenced by the amount of active sites on the catalyst and also by the dimension of the pores which slightly promoted a shape selective reaction. Above all, SZSBA-15 prepared with 15 wt% zirconia loading demonstrated the highest activity and show the highest shape selective effects with high degree of specificity due to its high surface acidity.

ACKNOWLEDGEMENTS

The authors acknowledge the financial support from Universiti Sains Malaysia under the Research University grants (814144 and 814181) and a TRGS grant (6762001). The first author also thanks the Ministry of Higher Education Malaysia for the financial support in the form of MyPhD.

REFERENCES

1. X. Wang, W. Xingguo, Q. Jin and T. Wang, *J. Am. Oil Chem. Soc.*, **90**, 1455 (2013).
2. M. K. Naik, S. N. Naik and S. Mohanty, *Catal. Today*, **237**, 145 (2014).
3. P. Y. Hoo and A. Z. Abdullah, *Chem. Eng. J.*, **250**, 274 (2014).
4. D. Singh, P. Patidar, A. Ganesh and S. Mahajani, *Ind. Eng. Chem. Res.*, **52**, 14776 (2013).
5. L. Wee, T. Lescouet, J. Fritsch, F. Bonino, M. Rose, Z. Sui, E. Garrier, D. Packet, S. Bordiga, S. Kaskel, M. Herskowitz, D. Farrusseng and J. Martens, *Catal. Lett.*, **143**, 356 (2013).
6. Y. C. Yang, S. R. Vali and Y. H. Ju, *J. Chin. Inst. Chem. Engrs.*, **34**, 617 (2003).
7. J. Ni and F. C. Meunier, *Appl. Catal. A Gen.*, **333**, 122 (2007).
8. Y. Liu, E. Lotero and J. G. Goodwin Jr., *J. Mol. Catal. A Chem.*, **245**, 132 (2006).
9. J. M. Marchetti and A. F. Errazu, *Biomass and Bioenergy*, **32**, 892 (2008).
10. M. I. Al-Widyan and A. O. Al-Shyoukh, *Bioresour. Technol.*, **85**, 253 (2002).
11. K. Saravanan, B. Tyagi and H. C. Bajaj, *Indian J. Chem.*, **53A**, 799 (2014).
12. T. H. Đặng and B. H. Chen, *Fuel Process. Technol.*, **109**, 7 (2013).
13. V. Simsek, L. Degirmenci and K. Murtezaoglu, *React. Kinet. Mech. Catal.*, **117**, 773 (2016).
14. J.n. Pérez-Pariente, I. Díaz, F. Mohino and E. Sastre, *Appl. Catal. A Gen.*, **254**, 173 (2003).
15. L. Hermida, A. Abdullah and A. Mohamed, *J. Porous. Mater.*, **19**, 835 (2012).
16. M. Kapoor and M. N. Gupta, *Process Biochem.*, **47**, 503 (2012).
17. C. A. Ferretti, A. Soldano, C. R. Apesteguía and J. I. Di Cosimo, *Chem. Eng. J.*, **161**, 346 (2010).
18. A. J. Chen, X. R. Chen and C. Y. Mou, *J. Chinese Chem. Soc.*, **57**, 820 (2010).
19. V. Degirmenci, D. Uner, B. Cinlar, B. Shanks, A. Yilmaz, R. Santen and E. M. Hensen, *Catal. Lett.*, **141**, 33 (2011).
20. S. Garg, K. Soni, G. M. Kumaran, R. Bal, K. Gora-Marek, J. K. Gupta, L. D. Sharma and G. M. Dhar, *Catal. Today*, **141**, 125 (2009).
21. M. H. M. Yusoff and A. Z. Abdullah, *J. Taiwan Inst. Chem. Eng.*, **60**, 199 (2016).
22. T. Geng, Q. Li, Y. Jiang and W. Wang, *J. Surfactants Deterg.*, **14**, 15 (2011).
23. Y. Sun, S. Ma, Y. Du, L. Yuan, S. Wang, J. Yang, F. Deng and F. S. Xiao, *J. Phys. Chem. B*, **109**, 2567 (2005).
24. C. K. Krishnan, T. Hayashi and M. Ogura, *Adv. Mater.*, **20**, 2131 (2008).
25. V. Degirmenci, Ö. Erdem, A. Yilmaz, D. Michel and D. Uner, *Catal. Lett.*, **115**, 79 (2007).
26. T. Alemdaroglu, *Commun. Fac. Sci. Univ. Ank. Ser. B*, **47**, 27 (2001).
27. L. Hermida, A. Z. Abdullah and A. R. Mohamed, *Chem. Eng. J.*, **174**, 668 (2011).
28. K. Barbera, P. Lanzafame, A. Pistone, S. Millesi, G. Malandrino, A. Gulino, S. Perathoner and G. Centi, *J. Catal.*, **323**, 19 (2015).
29. X. R. Chen, Y. H. Ju and C. Y. Mou, *J. Phys. Chem. C*, **111**, 18731 (2007).
30. K. Szczodrowski, B. Prélot, S. Lantenois, J. Zajac, M. Lindheimer, D. Jones, A. Julbe and A. van der Lee, *Micropor. Mesopor. Mater.*, **110**, 111 (2008).
31. B. Chang, J. Fu, Y. Tian and X. Dong, *Appl. Catal. A Gen.*, **437-438**, 149 (2012).
32. T. Witoon, T. Permsirivanich, N. Kanjanasoontorn, C. Akkaraphataworn, A. Seubsai, K. Faungnawakij, C. Warakulwit, M. Chareonpanich and J. Limtrakul, *Catal. Sci. Technol.*, **5**, 2347 (2015).
33. B. C. Gagea, Y. Lorgouilloux, Y. Altintas, P. A. Jacobs and J. A. Martens, *J. Catal.*, **265**, 99 (2009).
34. Y. Luo, Z. Mei, N. Liu, H. Wang, C. Han and S. He, *Catal. Today*, (2017), DOI:10.1016/j.cattod.2017.05.047.
35. K. Saravanan, B. Tyagi and H. C. Bajaj, *J. Porous. Mater.*, **23**, 937 (2016).
36. F. Azimov, I. Markova, V. Stefanova and K. Sharipov, *J. Univ. Chem. Technol. Metall.*, **47**, 333 (2012).
37. Y. Shao, L. Wang, J. Zhang and M. Anpo, *J. Phys. Chem. B*, **109**, 20835 (2005).
38. D. Zhang and J. Li, *Chin. Sci. Bull.*, **58**, 879 (2013).
39. V. K. Ivanov, A. Y. Baranchikov, G. P. Kopitsa, S. A. Lermontov, L. L. Yurkova, N. N. Gubanova, O. S. Ivanova, A. S. Lermontov, M. N. Rumyantseva, L. P. Vasilyeva, M. Sharp, P. K. Pranzas and Y. D. Tretyakov, *J. Solid State Chem.*, **198**, 496 (2013).
40. V. G. Deshmane and Y. G. Adewuyi, *Appl. Catal. A Gen.*, **462-463**,

196 (2013).
41. Y. Wang, J. Ma, D. Liang, M. Zhou, F. Li and R. Li, *J. Mater. Sci.*, **44**, 6736 (2009).
42. A. Z. Abdullah, Z. Gholami, M. Ayoub and F. Gholami, *Chem. Eng. Commun.*, **203**, 496 (2016).
43. I. Hashemizadeh and A. Z. Abdullah, *Online J. Sci. Technol.*, **2**, 47 (2012).
44. J. Barrault, S. Bancquart and Y. Pouilloux, *C. R. Chim.*, **7**, 593 (2004).